PERGAMON

Journal of South American Earth Sciences 16 (2003) 91–103

Journal of
South American
Earth Sciences

www.elsevier.com/locate/jsames

Thermal divide andesites–trachytes, petrologic evidence, and implications from Jurassic north Patagonian massif alkaline volcanism

Eugenio Aragón[a,b,*], Pablo Gonzālez[a,b], Yolanda E. Aguilera[b], Claudia E. Cavarozzi[a,b], Eduardo Llambias[a,c], Giorgio Rivalenti[c]

[a]*Centro de Investigaciones Geológicas, Calle 1 No 644 1900 La Plata, Argentina*
[b]*Facultad de Ciencias Naturales y Museo, UNLP. Paseo del Bosque S/N, 1900 La Plata, Argentina*
[c]*Dipartamento di Scienze della Terra, Universita degli Studi di Modena, Italy*

Received 1 May 2001; accepted 1 March 2003

Abstract

The Andesitas Alvar Formation is part of the large Jurassic volcanic province of Patagonia (southern South America) that, in Jurassic time, participated in the disassembling of Gondwana in a tensional–transtensional regime with large-scale half-grabens. This large igneous province contains alkaline and calc-alkaline series of andesite–trachyte, trachyte–rhyolite, and andesite–dacite trends. Four-phase experimental diagrams of Qz–Or–Ab–An and Ab–An–Ol–Di correlate with the TAS diagram and explain the Andesitas Alvar Formation's sodium-rich andesite–trachyte, which evolved through a thermal divide edge. This alkaline set initially included the paragenesis olivine–plagioclase–diopsidic augite, which was later replaced by hornblende–plagioclase–diopsidic augite. The andesite–trachyte trend is saturated in silica and rich in sodium and alumina. Diopsidic augite, plagioclase, and hornblende crystals are reverse zoned in magnesium, iron, calcium, and sodium, so the sodium-rich cores of plagioclase are not due to contamination, and the magmas mix several batches of partial melts of basic rock. Crystallization temperatures and pressures show that magma chamber emplacement and thermal reversal took place mainly at 4 kb. This is interpreted as the emplacement of collecting chambers at the brittle–ductile transition in the crust, where mixing and crystallization took place, followed by rapid extrusion in a transtensional tectonic environment.

Keywords: Alkaline; Andesite; Jurassic; Thermal divide; Trachyte

1. Introduction

The Andesitas Alvar Formation andesite–trachyte trend is part of a NW–SE stratovolcano belt in central northern Patagonia. This volcanism belongs to the Jurassic volcanic province of Patagonia (JVPP; Féraud et al., 1999), which includes 1,000,000 km^2 of lava, ignimbrite, and subvolcanic intrusions. The JVPP, one of the largest silicic provinces in the world, developed between the initial break-up of Gondwana, marked by the continental flood basalt province of Karoo–Antartica–Tasmania at 180–184 Ma (Heimann et al., 1994; Marsh et al., 1997), to the east, and the development of an active margin at 142–150 Ma (Haller and Lapido, 1980; Suarez et al., 1997; Féraud et al., 1999) to the west. During this 40 Ma span, volcanism migrated WSW (Féraud et al., 1999) through 650 km of the southern South American continental plate as part of the disassembling of Gondwana through an extensional to transtensional regime (Gust et al., 1985). The nature and style of the volcanism also show changes in time and space in Patagonia. In northern Patagonia, Aragón et al. (1996) describe three settings: a large, high-silica caldera field (178–183 Ma) to the east (Marifil Formation), the central Patagonia stratovolcano belt (160–174 Ma, Lonco Trapial Group), and a (active plate margin) volcanic arc (142–150 Ma, El Quemado Complex) to the west (Fig. 1).

The compositions of rocks from the JVPP range from alkaline to calc-alkaline. Haller et al. (1990), using TAS criteria, recognize alkaline trends for the trachytic-rhyolitic rocks (Marifil Formation) and calc-alkaline trends for the andesitic–dacitic rocks (Lonco Trapial Group). Rapela and Pankhurst (1993) classify the trachytic–rhyolitic trends

* Corresponding author. Address: Centro de Investigaciones Geológicas, Calle 1 No 644 1900 La Plata, Argentina.
E-mail address: earagon@cig.museo.unlp.edu.ar (E. Aragón).

0895-9811/03/$ - see front matter © 2003 Elsevier Ltd. All rights reserved.
doi:10.1016/S0895-9811(03)00046-4

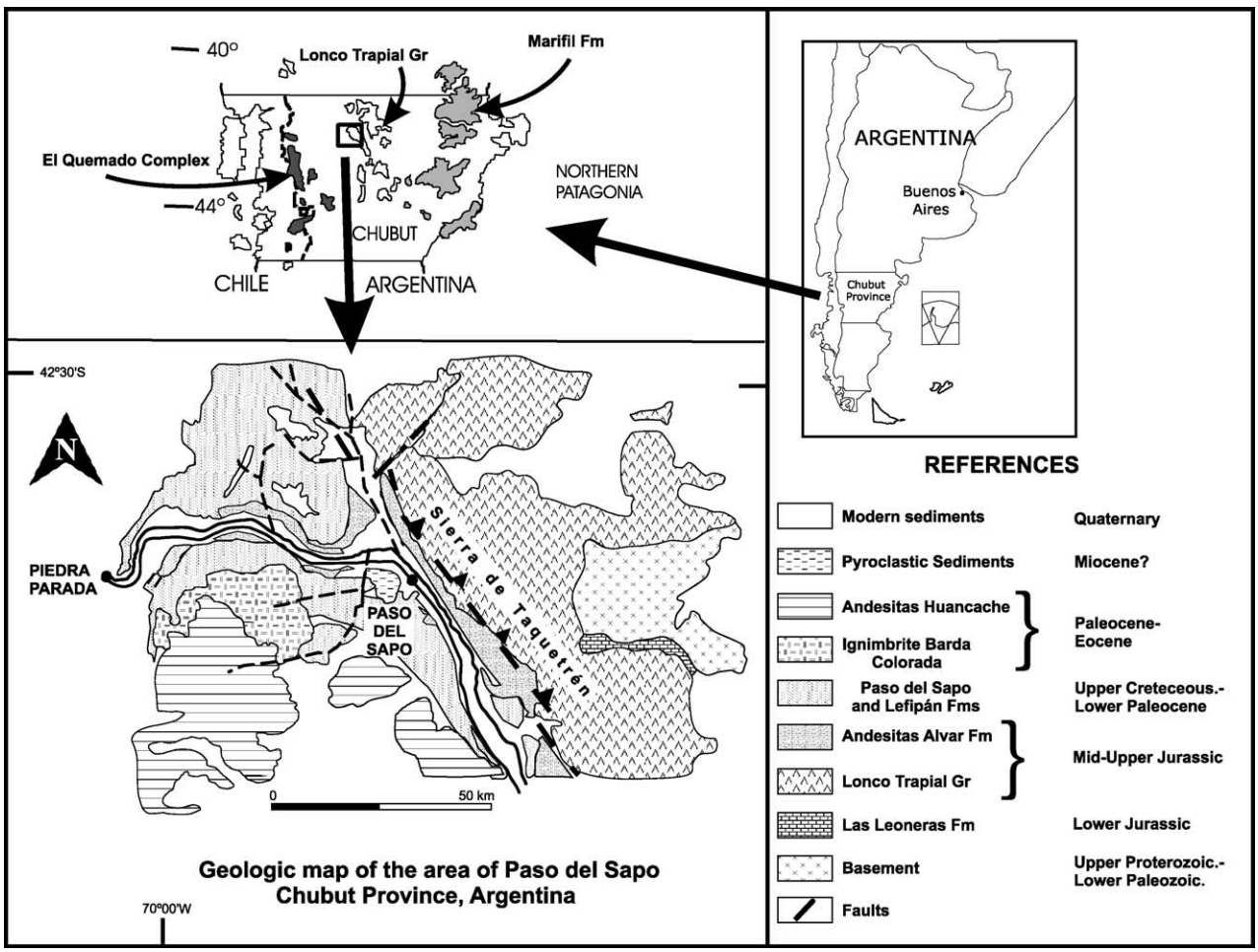

Fig. 1. Geology of Paso del Sapo area and location map.

(Marifil Formation) as alkaline-transitional, and Féraud et al. (1999) recognize calc-alkaline trends (Marifil Formation and Lonco Trapial Group).

In this work, we study outcrops east of the Lonco Trapial Group (Fig. 1), the Andesitas Alvar Formation, that have an andesitic–trachytic trend and evolved albite-rich trachyandesite–trachyte rocks.

To explain this peculiar trend of albite-rich trachytes, or the 'trachyte-syenite problem' (Morse, 1980, p. 247), we consider three possibilities: (1) the role of the thermal barrier, (2) the petrologic features of the Andesitas Alvar Formation, and (3) a reexamination of Beard and Lofgren (1991) experimental work on amphibolite melting.

Extensive discussion on the thermal divide (barrier) and the critical plane as a thermal divide has been provided by Yoder and Tilley (1962) and Morse (1980), who conclude that the Di–Ab–An–Ol system is close to a thermal barrier. However, Kushiro and Schairer (1970) highlight the imperfections of the diopside–plagioclase system as a thermal barrier.

The Andesites Alvar Formation demonstrates that fractional crystallization does not always drive liquids away from the critical plane but that liquids may evolve through it. In other words, liquids placed on a thermal divide have slopes not only toward nepheline or silica-rich valleys, but also along the edge, which runs parallel to both thermal valleys. Furthermore, this edge can be wide and coincides with the diopside–plagioclase–olivine cotectic on one side and the olivine-hypersthene cotectic for congruent melting conditions on the other (not for Ol–Hy peritectic conditions). The edge broadness is given by the stability of olivine, which tolerates silica (in magma) at ratios greater than the hypersthene composition. An increase in water enables the hornblende to replace olivine and hypersthene. The diopside–plagioclase–hornblende paragenesis persists over a wide range of pressure/temperature conditions (Beard and Lofgren, 1991; Beard et al., 1994; Patiño Douce and Beard, 1995) for sodium-rich experimental melts. The replacement of olivine by hornblende in the expanded critical plane and how it may affect the thermal divide has not been evaluated, but hornblende resembles olivine in silica consumption. A pressure increase allows for congruent melting of Hy for low water systems and favors incongruent melting for water-saturated systems (Kushiro,

Table 1
Petrographic characteristics of Andesitas Alvar Formation

	SR 1		SR 3		SR 4		SR 5		SR 6		SR 7	
	Pheno	Matrix	Pheno	Matrix	Pheno	Matrix	Pheno	Matrix	Pheno	Matrix	Pheno	Matrix
Plagioclase	X	X	X	X	X	X	X	X	X	X	X	X
Quartz							X			X (i)		
Olivine					X							
Clinopyroxene	X	X	X (2 g)	X	X		X		X		X (gl)	X (?)
Amphibole	X (2 g)	X	X	X	X		X		X		X	
Allanite		X										X
Apatite						X				X		
Zircon												
Opaque		X				X				X		
Lithics volc.												
Nodules					ol-px-op ± pg							
Alteration	se-cl-ca		se-sp		sp-cl-ca		ca		ca-ba		ba	
Texture	po-sd-mi		po-tr-sd		po-mif		po-se-pi		po-sd		gl-sd-pi	
Classification	Trachyte		Trachyte		Trachyandesite		Trachyte		Dacite		Trachyte	
	PA9901		PA9904		PA9905		PA1		PA4		PA6	
	Pheno	Matrix	Pheno	Matrix	Pheno	Matrix	Pheno	Matrix	Pheno	Matrix	Pheno	Matrix
Plagioclase	X	X	X	X	X	X	X	X	X	X	X	X
Quartz				X								
Olivine			X		X?	X	X		X		X?	
Clinopyroxene	X?				X		X	X(2 g)	X			X?
Amphibole	X		X	X	X		X		X			
Allanite												
Apatite		X										
Zircon						X						
Opaque		X		X		X	X	X	X	X	X	X
Lithics volc.			X									
Nodules	ol-pg				ol-px-op ± pg ± anph				ol-op			
Alteration	cl-ca		se-cl-ca		cl-ca-op		cl-ca-op		cl-ca		se-cl-ca	
Texture	po-pl		po-pl		po-pl		po-pl		po-pl-tr		po-pl-gl	
Classification	Andesite		Andesite		Andesite		Andesite		Andesite		Trachyandesite	

cl: chlorite, ca: calcite, sp: serpentinite, ba: bowlingite, ol: olivine, px: pyroxene, op: opaque, pg: plagioclase, po: porphiric, sd: seriated, mi: microlitic, br: breccia, tr: trachytic, pl: pilotaxitic, mif: fluid microlithic, gl: cumulophyric, y: inclusion, 2g: two generations.

1969; Chen and Presnall, 1975). We use an intermediate situation, such as dehydration melting, to reexamine Beard and Lofgren (1991) experimental data.

2. Analytical techniques

Rock chemical analyses were carried out at Activation Laboratories Ltd, Ontario, Canada. Major elements where analyzed by induced coupled plasma techniques. Trace and rare earth (REE) elements were analyzed by instrumental neutron activation analysis. Microprobe analyses of minerals were carried out at the Universitá degli Studi di Modena, Dipartamento de Scienze della Terra, Italy, on rocks with no alteration and clear phenocrysts. A JEOL electron microprobe with spectrometers, monochromatic radiation, and 5 nA and 15 Kv acceleration voltages with a focused beam was used for analysis. During analyses, Na and K were counted first. Na was counted 5 s to minimize Na loss; all other elements were counted for at least 20 s.

3. Geology

The time span between the eruption of the northern Patagonia Jurassic stratovolcano belts (Lonco Trapial Group and Andesitas Alvar Formation) and the easterly ignimbrite plateau (Marifil Formation) is restricted to 20 Ma. Plateau ignimbrites of the Marifil Formation have Rb/Sr ages ranging from 178 ± 1 to 183 ± 2 Ma (Rapela and Pankhurst, 1993) and Ar^{40}/Ar^{39} ages from 175.1 ± 0.5 to 187.4 ± 0.6 Ma (Féraud et al., 1999). Stratovolcano andesites of the Lonco Trapial Group overlie the Osta Arena Formation, which contains ammonite fossils of Toarcian age (Musacchio and Riccardi, 1971) and are overlain by olivine basalt (base of the Cañadon Asfalto Formation) with a K/Ar age of 173 ± 4 Ma

Table 2
Microprobe analyses of feldspars (0 = not detectable)

	Plagioclase						
	SR-6				SR-4		
	Pheno 1			Pheno 2	Pheno 1	Pheno 2	
	Rim	Core	Rim	Core	Core	Core	Rim
SiO2	56.36	58.52	54.68	56.75	66.25	63.76	62.59
Al2O3	30.54	28.89	31.03	29.4	22.11	23.88	22.92
TiO2	0.02	0.01	0	0.002	0	0	0.09
Cr2O3	0	0.04	0	0.04	0	0	0.05
MgO	0.004	0.04	0.03	0.01	0.03	0.10	0.56
NiO	0	0.02	0.05	0.01	0.08	0	0.05
FeO	0.25	0.25	0.37	0.32	0.14	0.33	1.12
MnO	0	0.02	0	0.03	0.03	0.03	0.04
CaO	9.65	8.28	10.41	8.36	0.46	1.79	3.03
Na2O	5.93	6.89	5.43	6.54	11.48	10.21	7.24
K2O	0.25	0.41	0.31	0.30	0.37	0.82	3.81
Total	103.0	103.37	102.31	101.76	100.95	100.90	101.48
Si	2.461	2541	2414	2505	2885	2775	2776
Al IV	1.539	1459	1586	1495	1115	1225	1224
Al VI	0.033	0.02	0.028	0.034	0.02	0	0
Ti	0.0006	0.0004	0	0.00007	0	0	0.003
Cr	0	0.002	0	0.001	0	0	0.002
Mg	0.0003	0.002	0.002	0.0009	0.002	0.062	0.037
Ni	0	0.0007	0.002	0.003	0.003	0	0.002
Fe (*)	0.009	0.009	0.014	0.012	0.005	0.012	0.042
Mn	0	0.0007	0	0.001	0.001	0.001	0.001
Ca	0.451	0.385	0.492	0.395	0.021	0.084	0.144
Na	0.502	0.58	0.465	0.559	0.97	0.861	0.623
K	0.014	0.022	0.018	0.017	0.02	0.045	0.216
Ab	51.9	58.8	47.7	57.6	95.9	87	63.4
An	46.6	39	50.5	40.7	2.07	8.5	14.6
Or	1.5	2.2	1.8	1.7	2.03	4.5	22

(Stipanicic and Bonetti, 1969). Andesitic volcanic rocks are also present beneath the Osta Arena Formation to the south (El Cordoba Formation) and above the Cañadon Asfalto Formation to the north, where the Taquetren and Andesitas Alvar Formations erupted at 161 Ma (K/Ar) and 165 Ma (Ar^{40}/Ar^{39}) (Féraud et al., 1999). This indicates that several andesitic cycles affected central Patagonia and that a spatial-temporal migration occurred from south to north (Nullo and Proserpio, 1975), similar to that of the Marifil Formation (Rapela and Pankhurst, 1993) but in a longer time span.

Page and Page (1993) conclude that the Lonco Trapial Group andesites, located NE of the Andesitas Alvar Formation (Fig. 1), belong to the eastern belt of a subduction-related Jurassic calc-alkaline magmatic arc.

Aragón and Mazzoni (1997) propose the name Andesitas Alvar Formation for the set of outcrops (sills and extrusive andesite) exposed at the Río Chubut between Piedra Parada and Paso del Sapo. Its age has been tentatively assigned to the early Paleocene-Late Cretaceous on the basis of a K/Ar age of a sill near Piedra Parada. The new K/Ar ages of plagioclase (K% 0.5907; error% 2.0078; Ar^{40} atm% 31.74; Ar^{40} Rad ccST/g 3.87) show that the extrusive andesites have a K/Ar age of 161.4 ± 7.3 Ma. Therefore, the Andesitas Alvar Formation is restricted to the extrusive andesites of Middle-Upper Jurassic age, which separates it from the sills correlated to the Tertiary volcanism present at the area as the Complejo Volcánico Piroclástico del río Chubut medio (Aragón and Mazzoni, 1997).

The Andesitas Alvar Formation is exposed for 70 km along the Rio Chubut valley (Fig. 1) and composed of andesitic lavas, autobreccias, and dikes. The base is not exposed, and the top of the unit is eroded to a subhorizontal surface, with a 1 m thick regolith of trachyandesite and andesite blocks with sandstone infilling overlain by the orthoquartzites of the Paso del Sapo Formation. These features are interpreted as a peneplain surface developed between the Late Jurassic and the Upper Cretaceous orthoquartzite sedimentation of the Paso del Sapo Formation.

4. Petrography

Andesitas Alvar Formation rocks are classified as andesites, trachyandesites, dacites, and trachytes according

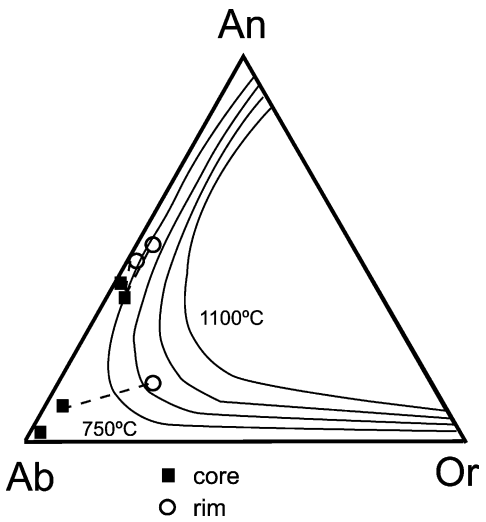

Fig. 2. An–Ab–Or diagram at 1 kb with 750, 900, 1000, and 1100 °C isotherms, after Fuhrman and Lindsley (1988). A line ties the core and rim of each phenocryst.

to the TAS diagram. The mineralogy includes plagioclase, clinopyroxene, amphibole, altered olivine, pyroxene, and accessory minerals in a devitrified groundmass (Table 1). The phenocryst sizes range from .5 to 10 mm. Groundmass is seriated and shows a microlitic texture from trachytic to pilotaxitic.

Andesite and trachyandesite have euhedral olivine and pyroxene phenocrysts altered to serpentine. A cumulophyric texture (amphibole-plagioclase) is present in the trachyandesites. A second generation of smaller phenocrysts of fresh clinopyroxene and amphibole may occur. Amphibole may have a strong resorption at the rim with exsolution of opaque minerals. Plagioclase phenocrysts are euhedral and subhedral, with poikilitic texture and strong zoning, and are oscillatory and patchy, so show a clear rim (not poikilitic) more calcitic than the core. Rims also show epitaxial growth of small subhedral plagioclases. Groundmass has a seriated pilotaxitic texture. Almost all andesites have rounded microgranular mafic nodules (up to 5 mm) of olivine + plagioclase ±

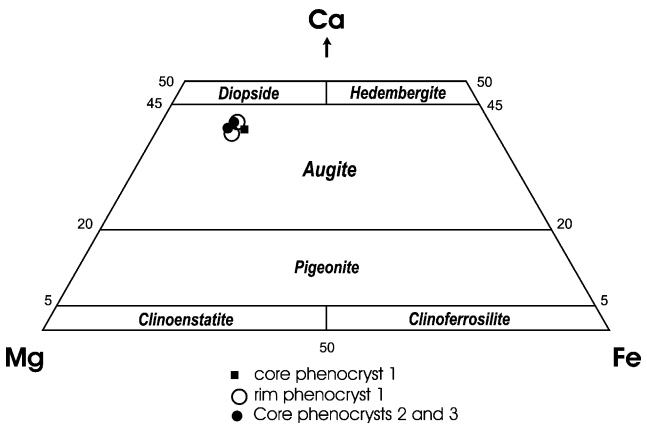

Fig. 3. Classification diagrams for Andesitas Alvar Formation clinopyroxenes, after Morimoto (1988).

Table 3
Microprobe analyses of pyroxenes (0 = not detectable)

	Pyroxene				
	SR-4				
	Pheno 1			Pheno 2	Pheno 3
	Rim	Core	Rim	Core	Core
SiO2	53.24	54.53	52.19	53.21	52.24
Al2O3	1.45	2.76	2.13	2.17	1.50
TiO2	0.32	0.62	0.48	0.51	0.37
Cr2O3	0.008	0	0	0.063	0
MgO	15.99	15.18	15.27	15.66	15.60
NiO	0.02	0	0.03	0.004	0
FeO	8.68	8.83	7.84	8.0	7.69
MnO	0.35	0.35	0.29	0.32	0.32
CaO	18.41	19.64	19.95	19.78	20.76
Na2O	0.33	0.38	0.36	0.34	0.28
K2O	0	0	0	0.13	0
Total	98.79	102.30	98.52	100.18	98.74
Si	1984	1964	1955	1959	1957
Al IV	0.026	0.036	0.045	0.041	0.043
Al VI	0.038	0.081	0.049	0.053	0.023
Ti	0.09	0.017	0.013	0.014	0.01
Cr	0.0002	0	0	0.002	0
Mg	0.889	0.815	0.853	0.86	0.871
Ni	0.0006	0	0.0008	0.0001	0
Fe (*)	0.271	0.266	0.246	0.246	0.241
Mn	0.011	0.011	0.009	0.01	0.01
Ca	0.735	0.758	0.801	0.78	0.833
Na	0.024	0.026	0.026	0.024	0.02
K	0	0	0	0.006	0
Mg	46.9	44.3	44.9	45.6	44.8
Fe	14.3	14.5	13	13.04	12.4
Ca	38.8	41.2	42.1	41.35	42.8

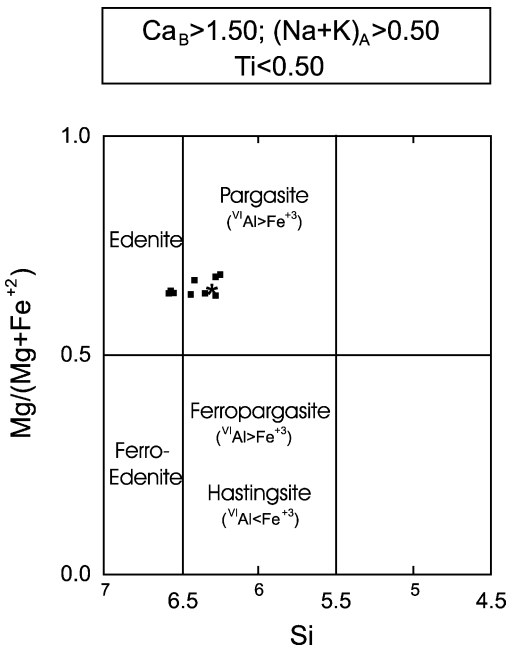

Fig. 4. Classification diagram of Andesitas Alvar Formation amphiboles, after Leake et al. (1997).

Table 4
Microprobe analyses of amphiboles (0 = not detectable, nd = not determined)

	Amphibole (Microprobe)									(Picking)
	SR-6						SR-4			PA9905
	Pheno 1			Pheno 2			Pheno 1			Pheno
	Rim	Ccore	Rim	Rim	Core	Rim	Rim	Core	Rim	
SiO2	44.56	43.46	44.93	45.36	45.71	45.52	44.03	44.66	43.43	43.37
Al2O3	11.16	11.29	10.51	9.91	9.80	10.05	11.06	11.11	11.01	13.77
TiO2	2.35	2.34	2.08	1.62	1.46	1.46	3.36	2.28	3.19	2.14
Cr2O3	0.05	0.02	0.02	0.056	0.08	0.04	0.06	0.05	0.04	0.0155
MgO	13.78	13.65	13.84	13.91	14.19	14.26	14.56	14.20	14.44	11.79
NiO	0	0	0	0.36	0.023	0.112	0.063	0	0.005	0.0078
Fe2O3	nd	nd	nd	nd	nd	nd	nd	nd	nd	6.66
FeO	13.78	13.81	13.89	13.30	13.85	13.8	12.08	12.29	12.11	5.50
MnO	0.28	0.24	0.26	0.28	0.22	0.34	0.20	0.22	0.25	0.14
CaO	11.08	10.68	10.66	10.05	9.99	9.73	11.10	10.13	10.16	10.34
Na2O	2.01	2.13	2.04	1.78	1.84	1.91	2.84	2.46	2.50	2.89
K2O	0.53	0.55	0.56	0.55	0.51	0.54	0.51	0.51	0.51	0.46
P2O5	nd	nd	nd	nd	nd	nd	nd	nd	nd	0.04
LOI	nd	nd	nd	nd	nd	nd	nd	nd	nd	2.07
Total	99.57	98.16	98.78	97.18	97.67	97.76	99.85	97.91	97.64	99.16
Si	6.34	6.27	6.43	6.57	6.58	6.55	6.25	6.41	6.27	6.31
Al IV	1.66	1.73	1.57	1.43	1.42	1.45	1.75	1.59	1.73	1.69
Al VI	0.21	0.19	0.20	0.26	0.24	0.25	0.10	0.30	0.15	0.67
Ti	0.25	0.25	0.22	0.18	0.16	0.16	0.36	0.25	0.35	0.23
Cr	0.005	0.002	0.002	0.006	0.009	0.005	0.007	0.006	0.004	0.002
Mg	2.92	2.94	2.95	3.00	3.04	3.06	3.08	3.04	3.11	2.50
Ni	0	0	0	0.04	0.003	0.013	0.007	0	0.0006	0.001
Fe (*)	1.64	1.67	1.66	1.61	1.67	1.66	1.43	1.48	1.46	1.32
Mn	0.03	0.03	0.03	0.03	0.03	0.04	0.02	0.03	0.03	0.02
Ca	1.69	1.65	1.64	1.55	1.54	1.5	1.69	1.56	1.57	1.61
Na	0.56	0.60	0.57	0.50	0.51	0.53	0.78	0.69	0.70	0.81
K	0.10	0.10	0.10	0.10	0.09	0.10	0.09	0.09	0.09	0.09
Mg × 100/(Fe + Mg + Mn)	63.59	63.37	63.56	64.61	64.25	64.24	67.89	66.93	67.56	65.10

pyroxene ± opaque ± amphibole. Nodule olivines are altered to serpentine, and at the contact, olivine-plagioclase crystals have developed simplectitic texture with exsolution of spinel. Nodules have a clinopyroxene, opaque corona.

Trachyte and dacite have euhedral-subhedral clinopyroxene and amphibole phenocrysts. Large clinopyroxenes are altered to serpentine, whereas smaller clinopyroxene phenocrysts are clear light green and show zoning. Small, rounded clinopyroxenes may form a corona around amphibole. Amphiboles are strongly pleocroic and poikilitic with small inclusions of plagioclase, apatite, and olivine. Larger phenocrysts usually show resorption at the rim with exsolution of opaque minerals. Plagioclase phenocrysts are euhedral and subhedral with pokilitic texture and zoning; they are also oscillatory and patchy with a clear rim (not poikilitic) more calcitic than the core. Rims may also show epitaxial growth of small subhedral plagioclases. Seriated groundmass has a trachytic texture. Trachyte may have accessory subhedral allanite crystals restricted to trachyte groundmass.

5. Mineral chemistry

Microprobe analyses on a trachyandesite (SR4) and a dacite (SR6) that are part of the andesitic cluster (Fig. 9D) were made. The trachyandesite has microgranular mafic nodules with simplectitic texture and amphibole-plagioclase aggregates with cumulophyric texture.

The plagioclase phenocrysts in the trachyandesites and dacites are fresh; a few crystals are slightly altered to sericite and seldom have calcite patches. Andesite plagioclases show increasing alteration to calcite. Phenocryst microprobe analyses (Table 2) show andesine to albitic composition with inverted zoning from Ab 58.8 at the rim to Ab 50.5 in the core. Some rims reach anorthoclase composition. A ternary diagram An–Ab–Or (Fig. 2) shows the reversal and how the most albitic cores are rimed by more calcic plagioclase or anorthoclase.

Most rocks have one or two pyroxene phenocryst generations. The first generation (present mainly in andesite) shows total alteration to serpentine. The second (present in all samples) is smaller and made up of clear

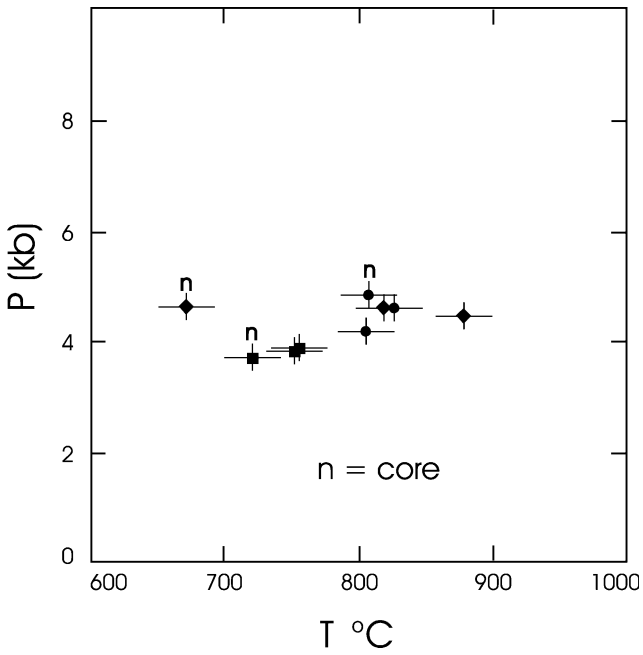

Fig. 5. Crystallization P/T diagram for plagioclase–amphibole core and rim pairs of the Andesitas Alvar Formation.

crystals that show zoning and are sometimes rimmed with oxides. Microprobe analyses (Fig. 3, Table 3) show that the later generation of clinopyroxenes is classified as QUAD containing augites of almost diopsidic composition with CaO contents of up to 20.75%. Zoning is mildly inverse, with cores richer in Fe and lower in Mg than are the rims.

Amphibole phenocrysts are strongly pleocroic, zoned, and of two generations. The first generation (in trachyte) is strongly oxidized on the rims and serpentinized. Elsewhere, it is poikilitic with plagioclase and apatite inclusions. Second-generation amphibole (in almost all samples) is smaller and fresh (in trachyte and trachyandesite), sometimes is slightly oxidized, and may show strong alteration. Rims can show epitaxial growth of small plagioclases or pyroxene coronas. Microprobe analyses of fresh amphibole (Fig. 4, Table 4) show that they are composed of pargasite–edenite, with CaO = 11.1% and Na_2O = 2.85%, and mildly inverse zoned with cores richer in Fe and lower in Mg than are the rims (altered amphiboles show oxide-rich rims).

Crystallization pressure was calculated after Johnson and Rutherford (1989) on the basis of Al content in amphibole. Crystallization temperatures were calculated after Holland and Blundy (1994) on the basis of the plagioclase-amphibole pair. Amphibole crystallization pressures fall close to 4 kb (3.71–4.82 ± 0.22 kb). Crystallization temperatures show an important reversal from core to rim and may reach 670 °C at the cores with 840 °C rims (Fig. 5). The reversal in crystallization temperature is consistent with the inverse compositional zoning of Mg, Fe, and Ca in pyroxenes and amphiboles and Ca and Na in plagioclase.

Olivine phenocrysts completely altered to bowlingite are distinguished by their prismatic forms. Accessory minerals are allanite, apatite, and scarce zircon. Allanite is restricted to the matrix with clear small euhedral crystals (epidote is not present). The opaque accessory mineral is ulvospinel (mineral formula Fe 0.90, Mg 0.06, Mn 0.03^2, TiO_4).

6. Rock chemistry

Variation diagrams of selected chemical analyses (Fig. 6, Table 5) are indicative of intermediate rocks with high Al_2O_3 and Na_2O contents and low K_2O. Rock classifications and silica saturations from the TAS diagram (Fig. 9D) show andesite, trachyandesite, dacite, and trachyte. Alumina saturation (Fig. 7) is of a metaluminous nature and evolves to a ratio close to 1.

The low SiO_2 and CaO and high Al_2O_3 contents in trachyandesites may be due to the inclusion of crystal fractionate aggregates, as evidenced by the cumulophyric texture of amphibole-plagioclase.

Normalized REE spidergrams (Fig. 8) show an enriched LREE against a depleted HREE with no Eu anomaly pattern. The increase in the LREE content and the La–Lu slope is related to the silica increase. The high LREE contents favor the appearance of allanite as an accessory mineral.

Normative minerals show small amounts of quartz, hypersthene, diopside, and sometimes olivine, always with an albite-rich plagioclase. These normative minerals have been plotted in the quaternary system of the silica-saturated part of the petrogenic residual system and in the expanded critical plane of the basalt system (Fig. 9A and B).

The behavior of the Andesitas Alvar Formation rocks in the Ab–An–Or–Qz diagram (Fig. 9A) clearly shows an evolution toward the thermal divide (Or–Ab tie line) instead of the thermal valley. Because these rocks have low (or no) normative Qz, they can be plotted in the Ab–An–Di–Ol diagram. In Fig. 9B, they follow a trend richer in plagioclase than that marked by the ternary cotectic at 1 kb. This trend fits the same ternary cotectic at higher pressures (note the migration of anhydrous eutectic at 5 kb in Fig. 9B).

7. Discussion

Mild reversals in the composition of the mineral phases (Pl, Ho, Di) modeled for thermometry and barometry show that thermal reversal took place during a deep-seated, 4 kb crystallization episode. No ascent stages are registered. Hibbard (1981) suggests that magma mixing generates textures due to cooling of the hotter magma and reheating of the cooler magma. Mixing textures, such as seriated groundmass, inverse zoning, patchy zoning, epitaxial growth of small plagioclase over plagioclase and amphibole

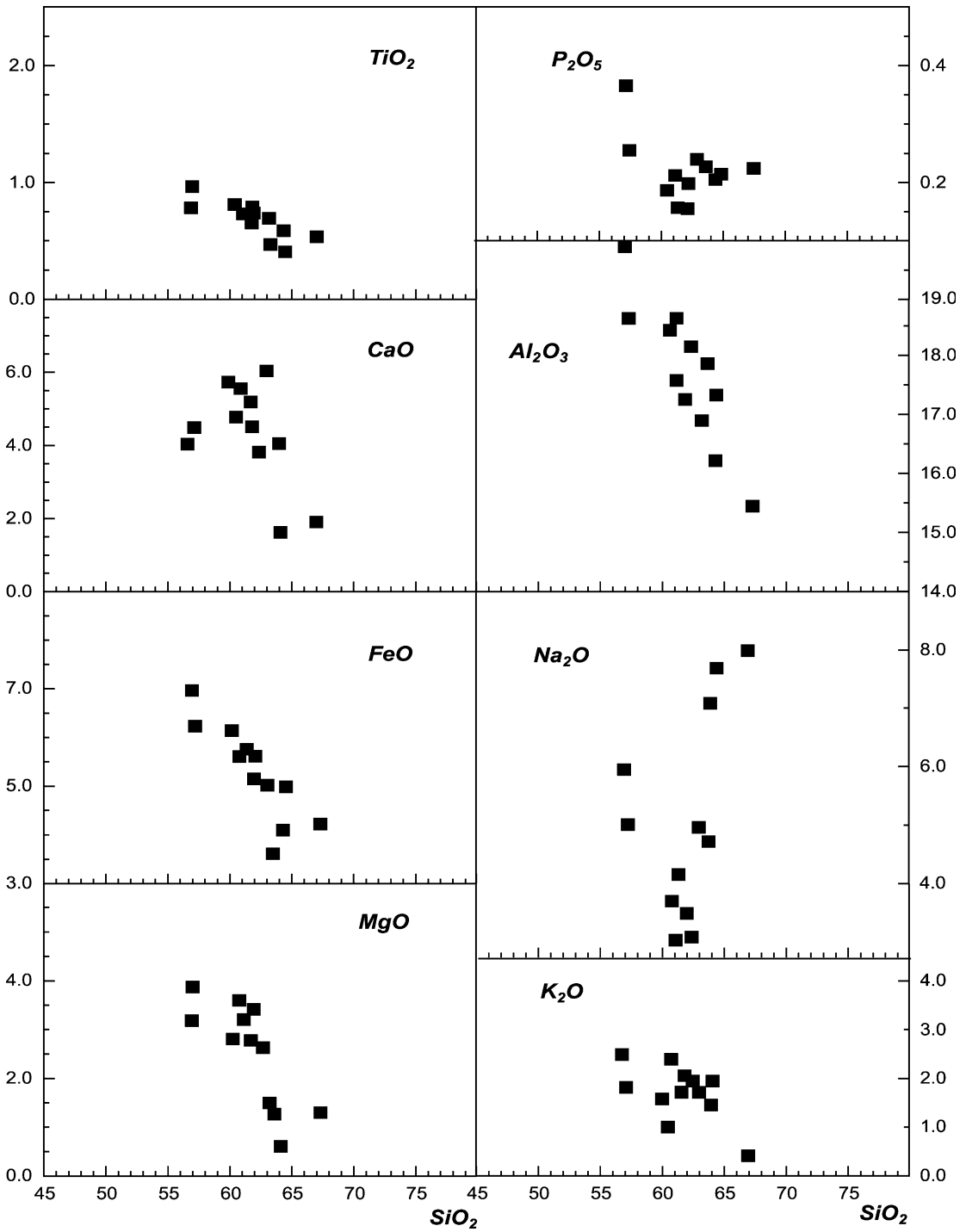

Fig. 6. Variation diagrams of Andesitas Alvar Formation major element compositions.

phenocrysts, amphibole with pyroxene coronas, and aggregates of plagioclase–amphibole phenocrysts, have been recognized in the Andesitas Alvar Formation. These compositional reversals and mixing textures suggest the coalescence of several partial melts, at a depth equivalent to 4 kb (15 km), into large collecting chambers. The cumulophyric texture (amphibole–plagioclase) in trachyandesite shows that crystal fractionation is also an important differentiation process in these large collecting chambers. These chambers were probably at the brittle–ductile transition of the crust, where crystallization took place followed by sudden extrusion. Reversals in the composition of the elements (Mg, Fe, Ca, and Na) exclude the possibility that albite-rich trachytes may be due to contamination. The depleted HREE pattern and lack of a positive or negative Eu anomaly are indicative of Ho–Pl fractionation at 4 kb (compensated Eu enrichment-depletion). Melting from a basic source is suggested by the presence of microscopic

Table 5
Mayor element analyses (0 = not detectable, nd = not determined, t = total iron)

	SR 1	SR 3	SR 4	SR 5	SR 6	SR 7
SiO2	62.74	60.97	55.49	62.58	61.64	65.59
TiO2	0.56	0.7	0.79	0.46	0.58	0.52
Al2O3	17.11	16.45	18.14	15.87	17.35	15.1
Fe2O3 t	5.51	5.41	6.87	4.34	3.68	4.53
MnO	0.05	0.06	0.12	0.07	0.2	0.04
MgO	1.24	2.49	3.74	0.57	1.31	1.24
CaO	1.87	4	4.67	4.21	6.26	2.11
Na2O	7.04	4.98	5.89	7.68	4.7	7.92
K2O	2.07	2.05	1.86	1.68	1.79	0.52
P2O5	0.21	0.22	0.25	0.2	0.21	0.22
LOI	2.22	3.18	2.54	31	2.88	1
Total	100.62	100.51	100.36	100.76	100.6	98.79
	PA9901	PA9904	PA9905	PA1	PA4	PA6
SiO2	57.24	57.95	56.71	55.39	58.93	54.30
TiO2	0.67	0.67	0.76	0.70	0.695	0.935
Al2O3	16.43	16.34	17.32	16.89	17.35	18.89
FeO	2.79	2.94	2.14	nd	nd	nd
Fe2O3	2.83	2.70	3.84	5.81 t	5.51 t	6.99 t
MnO	0.13	0.11	0.12	0.09	0.10	0.12
MgO	2.84	2.83	2.71	3.12	3.11	3.16
CaO	4.73	5.32	5.66	5.32	4.76	4.06
Na2O	3.82	3.23	3.46	2.76	2.97	4.89
K2O	2.24	1.90	1.52	1.02	1.88	2.34
P2O5	0.15	0.15	0.17	0.18	0.19	0.35
LOI	5.44	4.93	4.79	9.72	4.99	4.68
Total	99.30	99.10	99.20	100.99	100.49	100.71

mafic nodules with simplectitic olivine and scarce plagioclase.

These rocks may be classified as within the alkalic-subalkalic TAS discrimination limits. This circumstance is further complicated because they are intermediate to acid. To resolve this particular situation, we simultaneously use Ab–An–Or–Qz and Ab–An–Di–Ol diagrams (Fig. 9A and B) and plot their main cotectics on the TAS diagram (Fig. 9D). Fig. 9 shows how the petrogenetic residual system (at 1 atm), with its two minimums (mNe and mS) and its thermal divide (mThD), controls final composition trends (McBirney, 1984). Furthermore, if the basaltic critical plane cotectic is included (E–F line at 1 atm), the cotectic final stages (F) end at the thermal divide (mThD) of the petrogenic residual system. Note that, as pressure increases, the critical plane cotectic (E') moves toward more plagioclase-olivine-rich compositions (Fig. 9B), which is reflected in the TAS diagram (Fig. 9D) by movement to a position closer to the discriminating line between alkalic and subalkalic series. When thermal valleys of three ternary thermal divide systems, An–Ne–Qz, Di–Ne–Qz, and Fo–Ne–Qz, are plotted on the TAS diagram (Fig. 9D), the thermal valleys are at both sides of the expanded critical plane cotectic (E–F), suggesting that the cotectic runs along the edge of a thermal divide that separates the valley of the subsaturated systems from the saturated one. The broadness of the thermal divide edge with respect to silica enrichment for basaltic–andesitic liquids depends on the stability of Ol. Fig. 9D indicates that the cotectic Ol–En plane is the silica-saturated limit for the thermal divide edge. This cotectic Ol–En–Ab (point R in Fig. 9D) moves toward Ab composition (point F in Fig. 9D) as pressure increases (Fig. 10b). This move suggests that liquids with compositions between the Di–Ol–Plg cotectic and the Ol–Hy cotectic (not peritectic) will evolve to trachyte, across the TAS alkaline–subalkaline boundary line. In Ol–Hy peritectic conditions (high water pressure; Kushiro, 1974), liquids slide to the Opx–Cpx–Amph thermal valley that extends from basaltic andesites to rhyolite (calc-alkaline trend; McBirney, 1984, p. 323).

Because the expanded critical plane is a critically undersaturated system and the Ol–Hy cotectic is just saturated, liquids with these compositions seem to have more affinity for the alkaline series. Therefore, trends of igneous rocks that cross the subalkaline–alkaline discriminating limit of the TAS diagram and behave within the expanded critical plane or the Ol–Hy cotectic should be

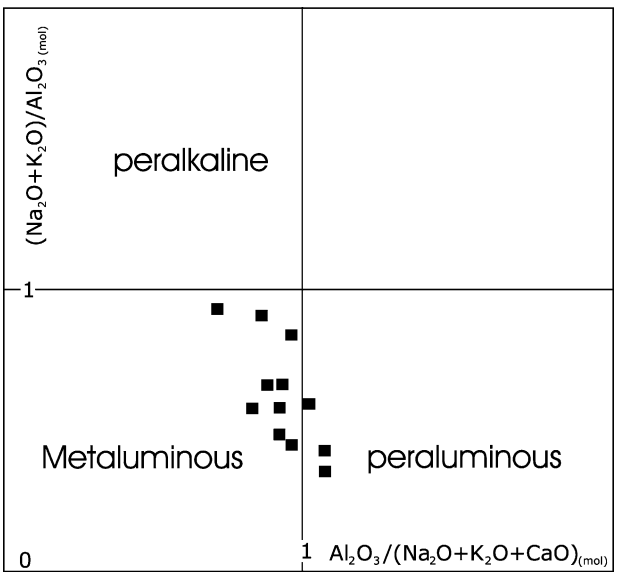

Fig. 7. Andesitas Alvar Formation alumina saturation diagram.

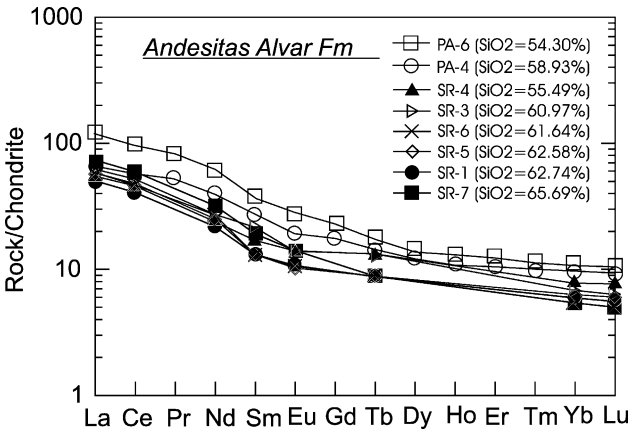

Fig. 8. Andesitas Alvar Formation chrondrite-normalized REE.

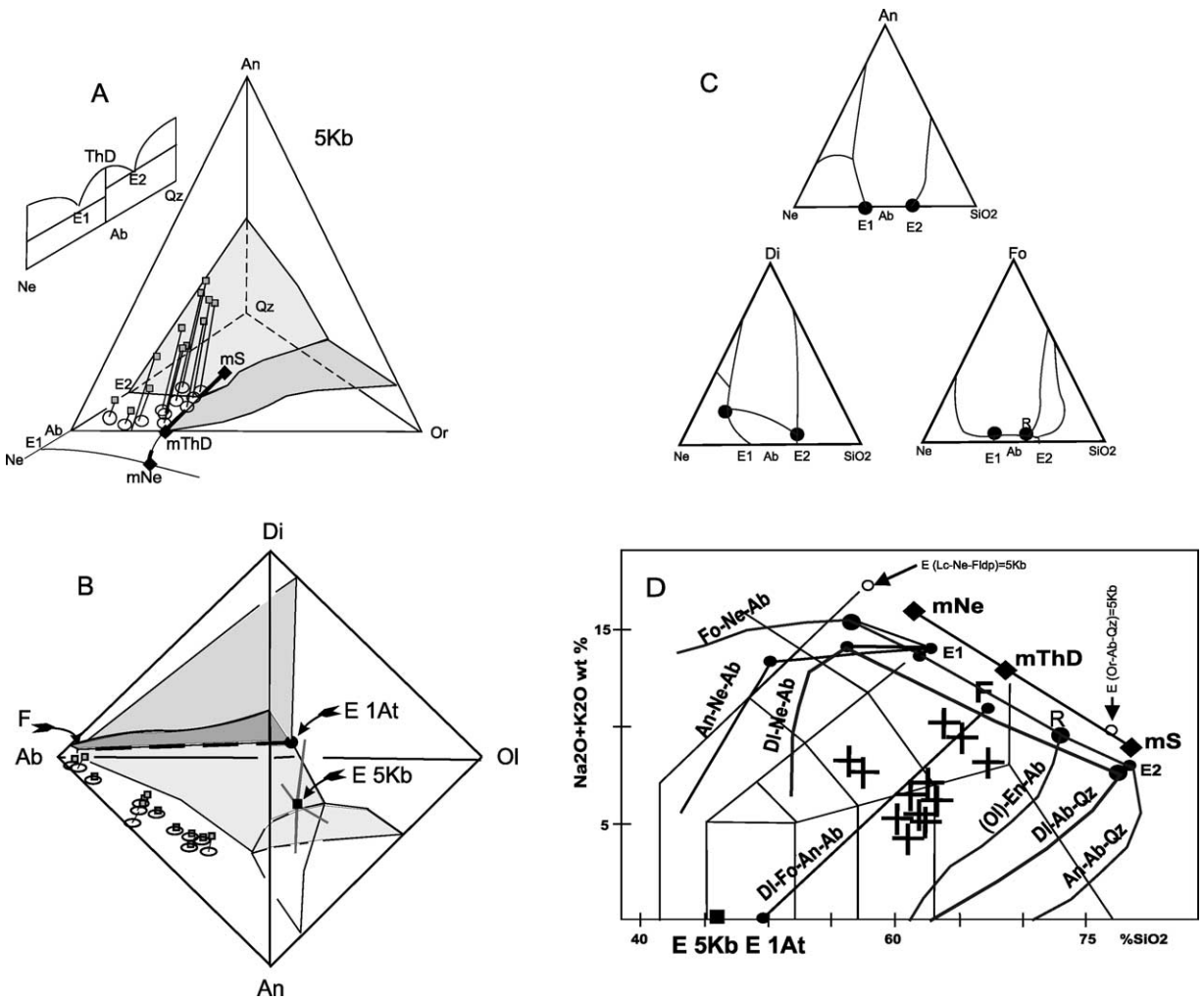

Fig. 9. Andesitas Alvar Formation plotted. (A) Granite system at 5 kb (Winkler, 1979). (B) Expanded critical plane (Yoder and Tilley, 1962), E5Kb after Presnall et al. (1978). (C) Simplified ternary phase diagrams of An–Ne–SiO_2, Fo–Ne–SiO_2, and Di–Ne–SiO_2 (Yoder and Tilley, 1962). (D) TAS diagram (Le Maitre et al., 1989) including simplified cotectics of A–C (recalculated to oxides from relative amounts of pure end members).

considered as alkaline or treated independently as a transitional series.

A further point must be discussed before classifying the Andesitas Alvar Formation as alkaline or transitional rocks using phase diagrams (critical plane): Hornblende has replaced olivine. Studies of partial melts of actinolitic- to amphibole-bearing basic to intermediate metamorphosed volcanic rocks under water-saturated and dehydration conditions (Beard and Lofgren, 1991) demonstrate that, in crustal conditions, the Ho–Di–Pl system is stable, and clinopyroxene and amphibole compositions are coincident with those in the Andesitas Alvar Formation (Figs. 3 and 4). This evidence indicates that Ho can be a part of the expanded critical plane (in place of olivine). This substitution will not affect the delicate silica mass balance of the expanded critical plane, because Ho and Ol use almost the same amount of silica.

Another point to consider is the possibility of liquids with these composition and petrological constraints. A reexamination of Beard and Lofgren's (1991) Table 3, which provides the experimental results for dehydration melting and water-saturated melting of five amphibolites, appears in Fig. 10a–c. Two trends of melts and minerals in equilibrium for dehydration melting are dependent of starting materials: (1) a trachytic–syenitic trend controlled by the olivine-hypersthene ± diopside ± plagioclase cotectic–peritectic and (2) a adakitic–throndjemitic trend controlled by the hypersthene-diopside ± plagioclase ± quartz cotectic (Fig. 10a). Water-saturated melting seems related to the hypersthene-diopside ± plagioclase ± quartz cotectic (Fig. 10a). The trachytic–syenitic trend suggests congruent melting for Opx at dehydration melting conditions.

The dehydration melting liquids of the trachytic–syenitic trend (Fig. 10a–c) are consistent with the Andesitas Alvar Formation composition. Furthermore, Fig. 10b includes, at the Andesitas Alvar Formation's Cpx–Ol–Ne–Qz tetrahedron, a projection from Cpx to the floor (Ol–Ne–Qz) that shows field boundaries for L (Fo–Opx) for a water-rich and water-poor bulk composition at

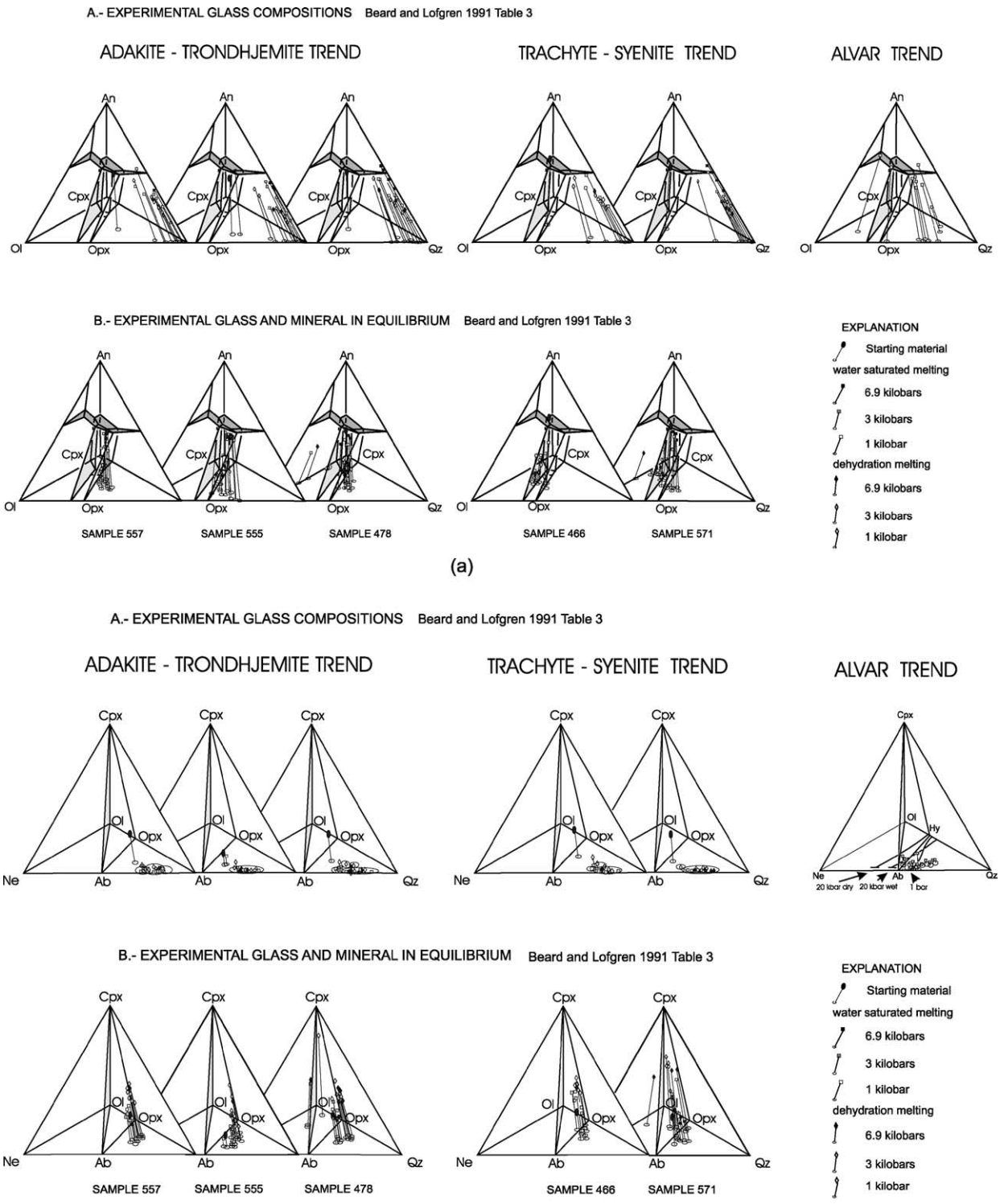

Fig. 10. The experimental results of Beard and Lofgren (1991) Table 3 compared with the Andesitas Alvar Formation. (a) Ol–An–Qz–Di tetrahedron showing the trace of phase relationships at 1 bar (modified from Presnall et al., 1979). (b) The basalt tetrahedron (Ol–Ne–Qz–Di). The Andesitas Alvar Formation trend includes L (fo-Opx) for both a water-rich bulk composition and a water-poor composition at 20 kbar total pressure (Kushiro, 1972) and for 1 bar (Bowen and Schairer, 1932). (c) The granite system (Ab–Or–An–Qz) (Winkler, 1979). The CIPW norms were calculated from glass compositions and glass and mineral mass balance using compositions of glass and mineral end members for Ab, An, Qz, Mt, and Il, hypersthene for Opx, paragasitic amphibole for Ho, and diopsidic augite for cpx.

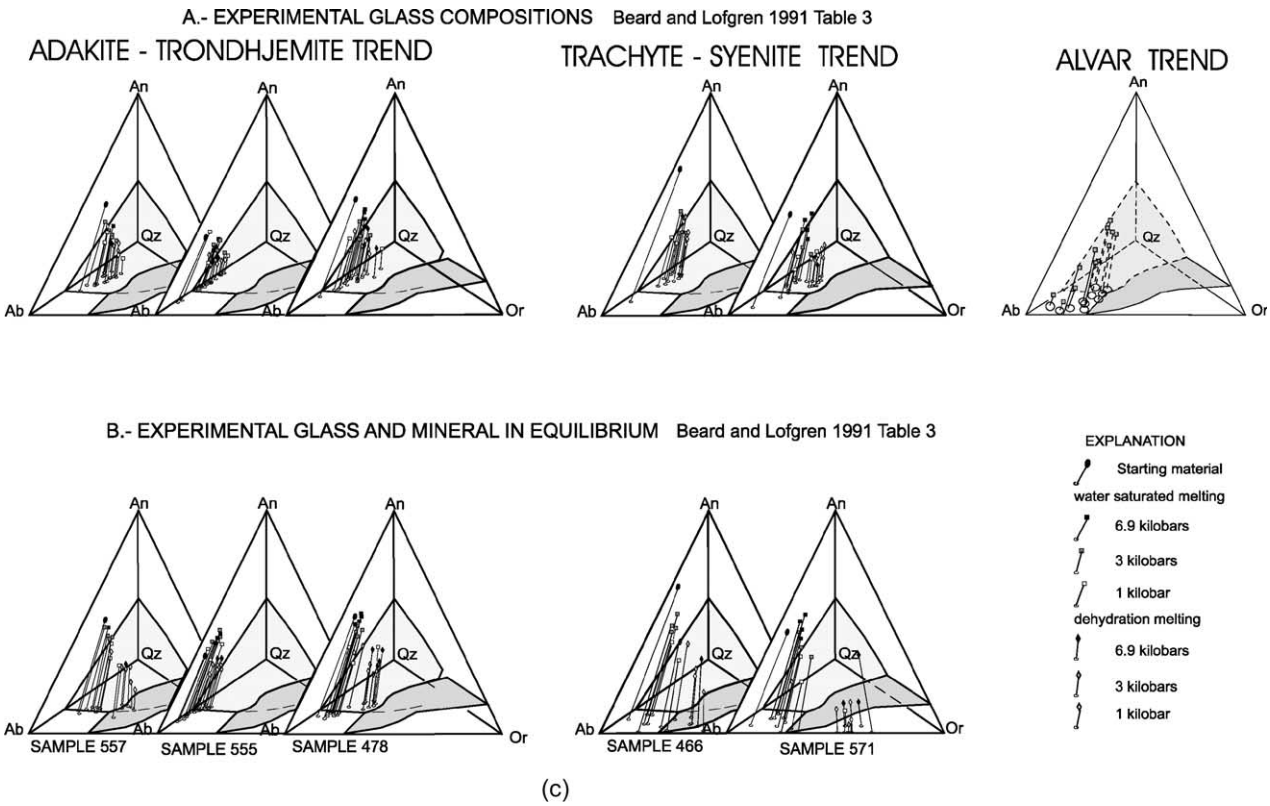

Fig. 10 (*continued*)

20 kbar and 1 bar total pressure (Kushiro, 1972). This shows how water-poor trends evolve from quartz-normative andesites to albite-rich trachytes. The most basic rocks of the Andesitas Alvar Formation have altered phenocrystals of olivine and pyroxene, which could account for the earliest generation paragenesis that, in the most evolved rocks, is replaced by Ho–Cpx–Plg. Unfortunately, there are no relict cores in altered pyroxenes to confirm it was orthorhombic.

8. Conclusions

The TAS diagram subalkalic-alkalic discrimination line lies close to the expanded critical plane ternary cotectic (Di–Ol–Plg) that runs along the thermal divide edge. As pressure increases and at dry conditions, this thermal divide edge is wide enough to include the Ol–Hy cotectic compositions (more or less the olivine tholeite field of the basalt tetrahedron). The Di–Ol–Plg and Ol–Hy cotectics will force liquids in this compositional field to cross the subalkalic–alkalic discrimination line and evolve to a trachyte composition. Water-saturated systems have a narrow thermal divide edge (Ho–Di–Plg system compositions), because at high (H_2O) pressure, enstatite changes the melting behavior from congruent to incongruent, thus destroying the thermal barrier in the dry system and enabling liquids of the olivine tholeite field to evolve to rhyolite compositions. Dehydration melting systems have much less water than water-saturated systems and seem to allow congruent melting of enstatite; thus, dehydration melting liquids in this compositional field (such as the Andesitas Alvar Formation) can be expected to evolve to trachyte.

The Andesitas Alvar Formation is a silica-saturated system that evolved to trachyte and therefore should be considered of alkaline nature or treated independently as a transitional series. Transitional series should be restricted to trends that evolve to trachyte through Di–Ol–Plg, Di–Ho–Plg, or Di–Hy–Ol–Plg equilibrium systems.

The magma chamber history shows the coalescence of partial melts at a depth equivalent to 4 kb (brittle–ductile transition in the crust). At this depth, the initial paragenesis of Ol–Di–Pl(Hy?) is replaced by Ho–Di–Pl, which causes further differentiation by crystal fractionation until extrusion is enabled.

Sudden extrusion of deep-seated magma chambers is considered evidence of rifting at a within-plate setting related to a transtensional stage that affected the southern South America continental area with large-scale NNW-SSE half-grabens. The Andesitas Alvar Formation is part of central Patagonia's stratovolcano belts of 160–174 Ma, one of the volcanic episodes that preceded the protracted breakup of Gondwana.

Further work should attempt to understand magma genesis (andesite–trachyte and rhyolite–trachyte trends) during

the breakup (30–40 Ma) of Gondwana, before true subduction to the west and seafloor spreading to the east developed.

Acknowledgements

We are grateful to Nancy Riggs who revised the english usage.

References

Aragón, E., Iñiguez Rodríguez, M.A., Benialgo, A., 1996. A Calderas field at the Marifil formation, new volcanogenic interpretation, Patagonian Massif, Argentina. Journal of South American Earth Sciences 9 (5/6), 321–328.

Aragón, E., Mazzoni, M.M., 1997. Geología y estratigrafía del complejo volcánico piroclástico del río Chubut medio (Eoceno), Chubut, Argentina. Revista de la Asociación Geológica Argentina 52 (3), 243–256.

Beard, J.S., Lofgren, G.E., 1991. Dehydration melting and water-saturated melting of basaltic and andesitic greenstones and amphibolites. Journal of Petrology 32 (2), 365–401.

Beard, J.S., Lofgren, G.E., Krishna Sinha, A., Tollo, R.P., 1994. Partial melting of apatite-bearing charnockite, granulite, and diorite: melt compositions, restite mineralogy, and petrologic implications. Journal of Geophisical Research 99 (B11), 21591–21603.

Bowen, N.L., Schairer, J.F., 1932. The system FeO–SiO_2. Amercan Journal of Science 5th Series 24, 177–213.

Chen, C.H., Presnall, D.C., 1975. The system Mg_2SiO_4–SiO_2 at pressures up to 25 kilobars. American Mineralogist 60, 398–406.

Féraud, G., Alric, V., Fornari, M., Bertrand, H., Haller, M., 1999. $^{40}Ar/^{39}Ar$ dating of the Jurassic volcanic province of Patagonia: migrating magmatism related to Gondwana break-up and subduction. Earth and Planetary Science Letters 172, 83–96.

Fuhrman, M.L., Lindsley, D.H., 1988. Feldspar minerals. American Mineralogist 73, 201–215.

Gust, D.A., Biddle, K.T., Phelps, D.W., Uliana, M.A., 1985. Associated middle to late Jurassic volcanism and extension in southern South America. Tectonophysics 116, 223–253.

Haller, M.J., Demichelis, A.H., Cabreros, J.B., Pardo, M.I., 1990. Litologia y geoquímica del vulcanismo Triasico-Jurásico en la Patagonia Extrandina y su relacion con el rifting Gondwanico. Actas, XI Congreso Geológico Argentino 1, 56–59.

Haller, M.J., Lapido, O.R., 1980. El Mesozoico de la Cordillera Patagonica Central. Revista de la Asociación Geologica Argentina 35, 230–247.

Heimann, A., Fleming, D.H., Elliot, K.A., Foland, A., 1994. A short interval of Jurassic continental flood basalt volcanism in Antarctica as demonstrated by Ar-40/Ar-39 geochronology. Earth Planet Scientific Letters 12, 19–41.

Hibbard, M., 1981. The magma mixing origin of mantled feldspars. Contributions to Mineralogy and Petrology 76, 158–170.

Holland, T., Blundy, J., 1994. Non-ideal interactions in calcic amphiboles and their bearing on amphibole-plagioclase thermometry. Contributions to Mineral Petrology 116, 433–447.

Johnson, M.C., Rutherford, M.J., 1989. Experimental calibration of the aluminum-in-hornblende geobarometer with application to Long Valley caldera (California) volcanic rocks. Geology 17, 837–841.

Kushiro, I., 1969. The system forsterite-diopside-silica with and without water at high pressures. American Journal of Science 267-A (Schairer volume), 269–294.

Kushiro, I., 1972. Effect of water on the composition of magmas formed at high pressures. Journal of Petrology 13, 311–334.

Kushiro, I., 1974. Melting of hydrous upper mantle and possible generation of andesitic magma: an approach from synthetic systems. Earth Planetary Science Letters 22, 294–299.

Kushiro, I., Schairer, J.F., 1970. Diopside solid solutions in the system diopside-anorthite-albite at 1 atm and at high pressures. Carnegie Inst. Washington Yearb. 68, 337–362.

Leake, B.E., Woolley, A.R., Arps, Ch.E.S., Birch, W.D., Gilbert, Ch.M., Grice, J.D., Hawthorne, F.C., Kato, A., Kisch, H.J., Krivovichev, V.G., Linthout, K., Laird, J., Mandarino, J.A., Maresch, W.V., Nickel, E.H., Rock, N.M.S., Schumacher, J.C., Smith, D.C., Stephenson, N.C.N., Ungaretti, L., Whittaker, E.J.W., Youzhi, G., 1997. Nomenclature of amphiboles: Report of the Subcommittee on Amphiboles of the International Mineralogical Association. Commission on New Minerals and Mineral Names. American Mineralogist 82, 1019–1037.

Le Maitre, R.W., Bateman, P., Dudek, A., Keller, J., Lameyre, J., Le Bas, M.J., Sabine, P.A., Schmid, J., Sorensen, H., Streckeisen, A., Woolley, A.R., Zanettin, 1989. A Classification of Igneous Rocks and Glossary of Terms. Recommendations of the International Union of Geological Sciences Subcommission on the Systematics of Igneous Rocks, Blackwell, London.

Marsh, J.S., Hooper, P.R., Rehacek, J., Duncan, R.A., Duncan, A.R., 1997. Stratigraphy and age of Karoo basalts of Lesotho and implications for correlations within the Karoo igneous province. In: Mahoney, J., Coffin, M.F. (Eds.), Large Igneous Provinces, pp. 247–272.

McBirney, A.R., 1984. Igneous Petrology, Freeman, Cooper & Company, San Francisco, 504 pp.

Morimoto, N., 1988. Nonmenclature of pyroxenes. Min. Mag. 52, 535–550.

Morse, S.A., 1980. Basalts and Phase Diagrams. An Introduction to the Quantitative Use of Phase Diagrams in Igneous Petrology, Springer, New York, 493 pp.

Musacchio, E.A., Riccardi, A.C., 1971. Estratigrafía principalmente del Jurásico, en la sierra de Agnia, Chubut, Rep. Argentina. Revista de la Asociación Geológica Argentina 26 (2), 272–273.

Nullo, F., Proserpio, C., 1975. La Formación Taquetren en Cañadón Zaino (Chubut) y sus relaciones estratigráficas en el ámbito de la Patagonia de acuerdo a su flora. Revista de la Asociación Geológica Argentina 30 (2), 133–150.

Page, R., Page, S., 1993. Petrologia y significado tectonico del Jarasico volcanico del Chubut central. Revista de la Asociación Geológica Argentina 48 (1), 41–58.

Patiño Douce, A.E., Beard, J.S., 1995. Dehaydration melting of biotite gneiss and quartz anphibolite from 3 to 15 kbar. Journal of Petrology 36 (3), 707–738.

Presnall, D.C., Dixon, S.A., Dixon, J.R., O'Donnell, T.H., Brenner, N.L., Schrock, R.L., Dycus, D.W., 1978. Liquidus phases relations on the join diopside-forsterite-anorthite from 1 atm to 20 kbar: their bearing on the generation and crystallization of basaltic magma. Contributions to Mineral Petrology 66, 203–220.

Presnall, D.C., Dixon, J.R., O'Donnell, T.H., Dixon, S.A., 1979. Generation of mid-ocean ridge tholeites. Journal of Petrology 20, 3–36.

Rapela, C.W., Pankhurst, R.J., 1993. El volcanismo riolítico del Noreste de la Patagonia: Un evento meso-jurásico de corta duración y origen profundo. Actas, XII Congreso Geológico Argentino y II Congreso de Exploración de Hidrocarburos 4, 179–188.

Stipanicic, P., Bonetti, M., 1969. Posiciones estratigráficas y edades de las principales floras jurásicas argentinas II. Floras doggerianas y málmicas. Ameghiniana 7 (2), 101–118.

Suarez, M., Marquez, M., de la Cruz, R., 1997. Nuevas edades del Complejo El Quemado a los 47°13′–47°22′ LS. Actas VIII Congreso Geológico Chileno, Antofagasta 2, 1552–1555.

Winkler, H.G.F., 1979. Petrogenesis of Metamorphic Rocks, fifth ed, Spriger, New York.

Yoder, H.S. Jr, Tilley, C.E., 1962. Origin of basalt magmas: an experimental study of natural and synthetic rock systems. Journal of Petrology 3, 342–532.